



Bidirectional single-multicore-fiber spatial channel network based on a spatial cross-connect and multicore EDFA that efficiently accommodates asymmetric data traffic

KYOSUKE NAKADA,¹ HITOSHI TAKESHITA,²  YUKI KUNO,³ YUSUKE MATSUNO,⁴ ITSUKI URASHIMA,¹ YUSUKE SHIMOMURA,² YUJI HOTTA,³ TSUBASA SASAKI,⁴ YUDAI UCHIDA,¹ KOHEI HOSOKAWA,² RYOHEI OTOWA,³ RIKA TAHARA,¹ EMMANUEL LE TAILLANDIER DE GABORY,²  YASUKI SAKURAI,³ RYUICHI SUGIZAKI,⁴ AND MASAHIKO JINNO^{1,*}

¹Kagawa University, 2217-20 Hayashi-cho, Takamatsu 761-0396, Japan

²NEC Corporation, 1753 Shimonumabe, Nakahara-ku, Kawasaki 211-8666, Japan

³santec Corporation, 5823 Ohkusa-nenjozaka, Komaki 485-0802, Japan

⁴Furukawa Electric Co., Ltd., 6 Yawata-kaigandori, Ichihara 290-8555, Japan

*jinno.masahiko@kagawa-u.ac.jp

Received 14 July 2023; revised 14 September 2023; accepted 28 September 2023; published 20 October 2023

In current wavelength division multiplexed (WDM) networks, capacity is deployed in a symmetrical manner, in which wavelength channels provide the same capacity in both directions. However, real data traffic in metro and backbone networks is observed to be considerably asymmetric resulting in wasted capacity in an under-loaded direction. This data traffic asymmetry is expected to increase further in the forthcoming Beyond 5G era due to newly emerging bandwidth-hungry services based on cloud computing. In such a situation, the wasted link capacity in the under-loaded direction can no longer be overlooked. In this paper, we propose a single-multicore-fiber (MCF) bidirectional spatial channel network (SCN) architecture that efficiently accommodates up and down asymmetric traffic. We present a proof-of-concept demonstration of the asymmetric bandwidth allocation in a single-MCF SCN by constructing a single-MCF bidirectional ring network testbed that comprises two spatial cross-connects based on 19-core fiber core selective switches with an $M \times N$ wavelength-selective switch and a bidirectional 7-core erbium-doped fiber amplifier with reversible optical isolators. Experimental results for bit error rate measurements of WDM optical signals traveling through different cores in different directions show there is almost no optical signal-to-noise ratio penalty for transmission through the single-MCF bidirectional ring network testbed. © 2023 Optica Publishing Group

<https://doi.org/10.1364/JOCN.499998>

1. INTRODUCTION

There are two major differences between optical access networks and other optical networks (metro, core, and submarine networks). First, the former employs links comprising a single single-mode fiber (SMF) that is shared by upstream and downstream traffic, while the latter employs links comprising a pair of SMFs, each of which is dedicated to upstream and downstream traffic. Second, in the former, the uplink and downlink data rates are generally different and change dynamically; however, in the latter they are the same and fixed [1]. The reasons for this may be that the number of access system fibers is huge, so there is a strong economic dynamic to halve the number of fibers by sharing them between upper and lower traffic,

and traffic asymmetry is tolerated by sharing fibers. Another possible reason is that the volume of uplink and downlink traffic changes greatly depending on the service that clients use; however, this traffic asymmetry is expected to be flattened by the statistical multiplexing effect as traffic aggregates in metro and core networks.

Unfortunately, non-negligible traffic asymmetry is observed in Internet protocol (IP) backbone networks [2]. The authors of [2] defined the symmetry ratio of connection ρ as the ratio of the peak bit rates for the low- and high-load propagation directions on each link (ρ will be between 0 and 1, $\rho = 0$ for a link with traffic flow in only one direction, and $\rho = 1$ for a link with identical traffic). They observed a large US IP-backbone network with 57 IP link pairs between routers and found

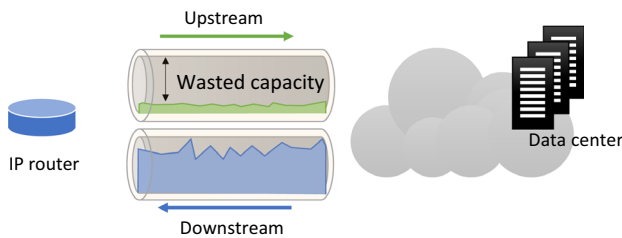


Fig. 1. Inefficient accommodation of asymmetric traffic in the current IP network.

that the symmetry ratio of the network, which is obtained by weighting the link symmetry ratio with the amount of traffic on each link, is 0.5. In the forthcoming Beyond 5G era, the progress in cloud computing may further increase traffic asymmetry [3].

Figure 1 shows an image of the inefficient accommodation of asymmetric traffic in the current IP network. In such a situation, the wasted link capacity in the under-loaded direction can no longer be overlooked, especially in submarine optical cable systems where the number of fibers accommodated in a cable is limited. An initial study that explored the possible benefits of asymmetric optical connections was reported in the early 2010s and found that using unidirectional circuits to establish asymmetric connections can provide significant cost savings [2]. To the best knowledge of the authors' knowledge, since then, there have been few studies that investigated asymmetric optical networks [2–5].

On the other hand, steady progress has been made in both the wavelength division multiplexing (WDM) layer, such as bandwidth variable transceivers (BVTs) [6,7] and highly flexible reconfigurable optical add/drop multiplexers [8], and spatial division multiplexing (SDM) layer, such as multicore fibers (MCFs) [9], multicore erbium-doped fiber amplifiers (MC-EDFAs) [10], and spatial channel networks (SCNs) [11] based on spatial cross-connects (SXC) [12] that employ core selective switches (CSSs) [13]. Here, the SCN is a scalable and economical optical network architecture in the forthcoming SDM era, where the current optical layer evolves into hierarchical WDM and SDM layers, while an optical node is decoupled into an SXC and a conventional wavelength cross-connect (WXC) to form a hierarchical optical cross-connect [12]. A spatial channel (Sch) is a media channel in the SDM layer that is constructed by connecting cores in each SDM link (an MCF or parallel SMFs) on a route using SXCs. If an aggregate demand between a source/destination node pair is comparable to the capacity of a single-mode core, an Sch is established between the source/destination node pair bypassing overlying WXCs using large scale, low-cost, and low-loss SXCs. These areas of progress motivated us to investigate SCNs that can efficiently accommodate asymmetric IP traffic by employing such recent advances. Among telecommunications network segments, submarine optical cable networks are one of the most likely segments where SDM technology will be applied first, as they are designed under a limited cable space constraint. We believe that the proposed technology is well suited to this segment where cable space is limited and core resources are precious because it can mitigate the wasted bandwidth problem of asymmetric traffic. As this technology matures, we

expect that its application area will expand from point-to-point submarine cable systems to regional submarine cable networks including bidirectional branching units with core granularity switching functionality and metro core networks comprising bidirectional SXCs.

In this paper, we propose a single-MCF SCN architecture that has bidirectional links comprising a single MCF and that efficiently accommodates up and down asymmetric traffic. We present a feasibility demonstration of the asymmetric bandwidth allocation in a single-MCF SCN by constructing an SCN testbed comprising bidirectional SXC and MC-EDFA prototypes. This paper is an expanded version of [14] with additional detailed descriptions of MCF-based optical devices used in the testbed: (i) an any-core-access CSS line-side module, where packaged CSS and core selector (CS) prototypes are equipped into a 19-inch rack mount case; (ii) a 19-core fiber (19-CF) employed in the CSS and CS prototypes, which is an MCF with 19 cores in the cladding designed so as to have a sufficiently suppressed higher-order mode even in a shorter (~ 1 m) length; and (iii) a bidirectional MC-EDFA prototype that has the capability to reconfigure independently the amplification direction of a WDM signal for each core.

The rest of this paper is organized as follows. Section 2 details our concept for efficiently accommodating asymmetric IP traffic in a bidirectional single-MCF SCN. Section 3 describes the functionalities and characteristics of each building block of a bidirectional single-MCF SCN: a CSS, CS, $M \times N$ wavelength selective switch (WSS), and bidirectional MC-EDFA. Section 4 presents proof-of-concept demonstration results for the bidirectional single-MCF SCN testbed including bit error rate (BER) measurements of routed SDM optical signals. Section 5 presents our conclusions.

2. BASIC CONCEPT BEHIND EFFICIENTLY ACCOMMODATING ASYMMETRIC TRAFFIC USING A SINGLE-MCF LINK

This section describes the basic concept of how a single-MCF bidirectional SCN efficiently accommodates asymmetric traffic. First, assume that two unidirectional SMF pairs accommodate upstream or downstream optical signals multiplexed in the WDM layer using a $1 \times N$ WSS as shown in Fig. 2. If each SMF has a total capacity of 20 Tb/s, client IP routers require an asymmetric bandwidth of 10 Tb/s for the downstream bandwidth and 3.3 Tb/s (1/3 of the downstream) for the upstream bandwidth, and the same capacity of 10 Tb/s is allocated to both directions using a conventional fixed bandwidth optical transmitter (Tx) and receiver (Rx). The traffic asymmetry results in the wasted link capacity of 6.6 Tb/s in the less busy upstream direction.

This capacity waste can be mitigated by introducing an $M \times N$ WSS, a fan-in fan-out (FIFO) device, a single-MCF with four cores in the cladding [hereafter referred to as a four-core fiber (4-CF)], a bandwidth variable optical transmitter (BV-Tx), and a bandwidth variable optical receiver (BV-Rx) as shown in Fig. 3. Here, an $M \times N$ WSS is a type of WSS that has M input SMF ports and N output SMF ports, whereas a typical WSS has one input SMF port and N output SMF ports ($1 \times N$ WSS). A FIFO device has a single-input MCF

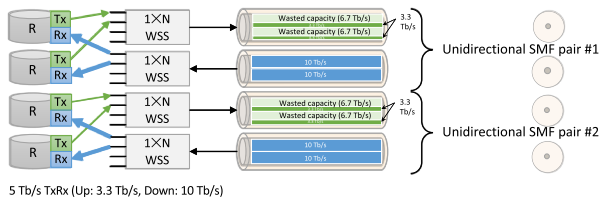


Fig. 2. Conventional symmetric capacity allocation in the up and down directions.

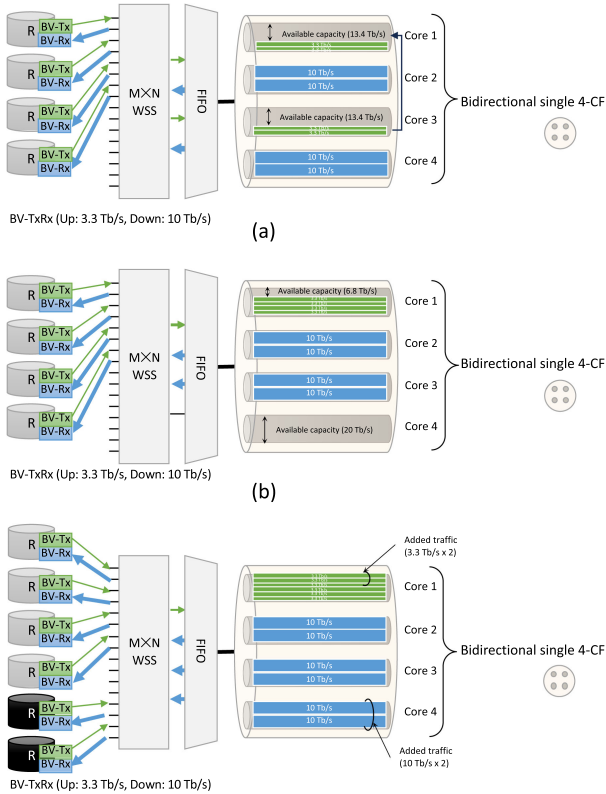


Fig. 3. Basic concept behind the proposed asymmetric capacity allocation scheme.

with C cores and C output SMF ports and provides spatial multiplexing and demultiplexing functions. The $M \times N$ WSS and FIFO device are reciprocal devices and can be used by changing the propagation direction per port. An optical signal launched into any of the M input ports of the $M \times N$ WSS can be switched to any of the N output ports and vice versa. A BVT, which comprises a BV-Tx and BV-Rx, is an optical transceiver that supports multiple baud rates or multiple numbers of subcarriers to provide the required bandwidth. The capability for generating multiple adjacent optical subcarriers can be achieved by employing multiple optical transceivers integrated on a single monolithic chip or a single coherent transceiver combined with advanced digital signal processing to transform a single carrier wavelength into multiple lower-bandwidth digital subcarriers.

Using these new technologies, a cohesive amount of available free capacity can be secured by cramming another upstream traffic flow into the free capacity of a core allocated for the upstream. This enables us to accommodate additional

clients having similar asymmetric traffic as explained in detail below. The BVT discussed here is supposed to have an ability to generate an optical signal at any center frequency with the minimum spectral width necessary to meet the respective traffic demand independently for the uplink and downlink. Since an $M \times N$ WSS can output any spectrum at any input port to any output port, the two 3.3-Tb/s optical signals (shown in green) in core 3 in Fig. 3(a) can be packed into the free capacity of core 1. As a result, the free spectrum that has been fragmented in each core in Fig. 3(a) can be combined into a large chunk, as shown in Fig. 3(b). This free capacity can accommodate, for example, optical signals for two clients with the same asymmetric traffic, as shown in Fig. 3(c).

Of course, a combination of an $M \times N$ WSS and four SMFs can also provide similar capability to accommodate asymmetric traffic efficiently. However, it should be emphasized that since an MCF has multiple cores in a single cladding and the direction of optical signal propagation through each core is arbitrary, our solution is more consistent with the proposed asymmetric traffic accommodation scheme than the solution using multiple SMFs. As discussed below, the advantages of using MCFs are further enhanced by the ability to employ bidirectional cladding-pumped MC-EDFAs. An $M \times N$ WSS can be formed by connecting $M1 \times N$ WSSs and $N1 \times M$ optical switches. The $1 \times N$ WSSs could be replaced with $1 \times N$ splitters (SPLs) to form an $M \times N$ multicast switch (MCS) if used with coherent transponders.

3. COMPARISON BETWEEN PROPOSED BIDIRECTIONAL SINGLE-MCF SXC AND CONVENTIONAL DUAL-MCF UNIDIRECTIONAL SXC ARCHITECTURES

This section discusses how to extend the concept described above in Section 2. To this end, the conventional dual-MCF unidirectional SXC configuration is first described and then compared to the proposed bidirectional single-MCF SXC architecture.

A. Conventional Dual-MCF Unidirectional SXC Architecture

Figure 4(a) shows a conventional 3-deg SXC architecture based on $1 \times N$ CSSs with an MCF-pair per degree. In this architecture, an ingress and egress CSS pair and its associated MC-EDFA pair are placed at each node degree. Here, a CSS has a one input MCF port and N output MCF ports [12,13,15] as shown in Fig. 4(b) and provides the functionality to switch an optical signal launched into any core in the input MCF to a core that has the same core identifier of any output MCF. Two of the N ports of the CSS are used for cross-connects between links (west, north, and south), and the remaining ports are used to add or drop signals arriving at or departing from this location. In order to achieve the any-core-access capability, a CS is placed at each add/drop port. A CS has one input MCF port and one output SMF port [12,15] as shown in Fig. 4(c) and provides the functionality to switch an optical signal launched into the SMF port to any core of the MCF port. Since each $1 \times N$ WSS, which multiplexes

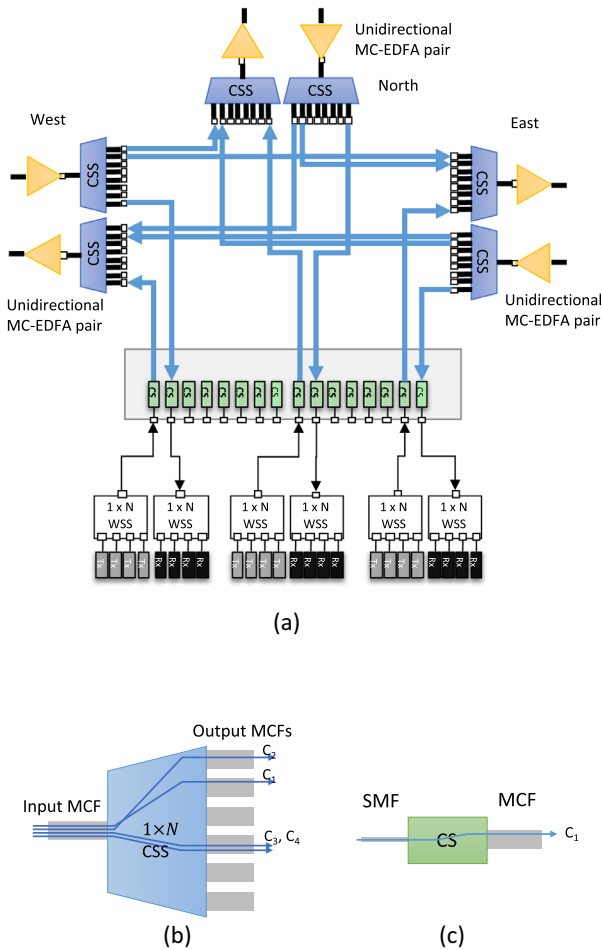


Fig. 4. Conventional dual-MCF unidirectional SXC and its key building blocks. (a) Conventional dual-MCF unidirectional SXC. (b) CSS. (c) CS.

or demultiplexes optical signals in the WDM layer, is connected to a CSS dedicated to a specific direction via a CS, this SXC architecture has the add/drop part connection flexibility capabilities of any-core-access and directional.

B. Proposed Single-MCF Bidirectional SXC

Figure 5(a) shows the proposed single-MCF bidirectional SXC architecture that comprises CSSs, CSs, $M \times N$ WSSs, BVTs, and bidirectional MC-EDFAs.

Similar to the FIFO device and $M \times N$ WSS, the CSS and CS are reciprocal devices and can be used by changing the propagation direction for each core. Each CSS in the SXC can connect any core in the line side MCF to the core with the same core number in the line side MCF in the other direction, or to any CS on the client side, regardless of the propagation direction of the optical signal in the core. The SXC has the add/drop part connection flexibility capabilities of any-core-access and directional the same as the dual-MCF unidirectional SXC described in the previous section. An optical signal sent from a transmitter connected to any client port of the $M \times N$ WSS can be multiplexed into any core in the MCF of the CSS to which the $M \times N$ WSS is connected. Similarly, an optical signal coming through any core of the MCF of the CSS can

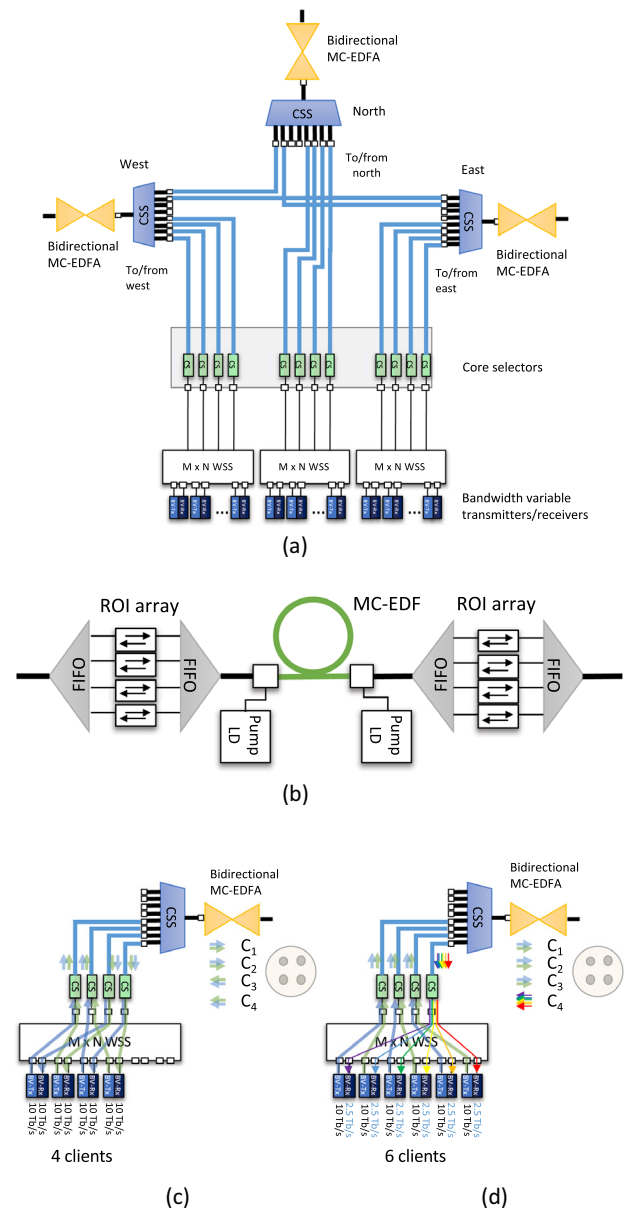


Fig. 5. Single-MCF bidirectional SXC. (a) Proposed single-MCF bidirectional SXC. (b) Cladding-pumped MC-EDFA with variable amplification direction for each core. (c) Symmetric bandwidth allocation. (d) Asymmetric bandwidth allocation.

be received by a receiver connected to any client port of the $M \times N$ WSS.

A bidirectional MC-EDFA that has the capability to reconfigure independently the amplification direction of a WDM signal for each core. Such a bidirectional MC-EDFA can be constructed by combining a bidirectional cladding-pumped MC-EDFA [10] and reversible optical isolators (ROIs) via an MCF FIFO device as shown in Fig. 5(b). Here, an ROI is an optical isolator whose transmittable direction can be changed using a 1×2 optical switch and an optical circulator.

By using a single MCF and a single CSS as a bidirectional link and a bidirectional core switch, respectively, and by introducing a novel bidirectional MC-EDFA, the proposed single-MCF bidirectional SXC mitigates the capacity waste

for asymmetric traffic in conventional optical networks. Figures 5(c) and 5(d) show how a single-MCF bidirectional SXC can efficiently accommodate asymmetric traffic. In the figures, only 1 deg of the SXC in Fig. 5(a) is depicted for simplicity. We assume the use of BVTs whose Tx and Rx bandwidths can be changed independently. Let us assume that (i) the capacity of each core of the MCF is 20 Tb/s, (ii) the transmission rate variable range of the BVTs is 2.5 Tb/s to 10 Tb/s with a 2.5-Tb/s step, and (iii) the number of usable cores for adding and dropping at this node is four. If clients require a 10-Tb/s bandwidth for both the upstream and downstream (symmetrical traffic), two 10-Tb/s signals can be multiplexed into a core in the WDM layer using the $M \times N$ WSS. As a result, four clients can be accommodated using the available four cores as shown in Fig. 5(c). On the other hand, if clients require a 10-Tb/s bandwidth for the upstream and a 2.5-Tb/s bandwidth for the downstream (asymmetric traffic), the accommodable number of clients increases from four to six, because one core among the four cores can be shared by six 2.5-Tb/s downstream optical signals that have a reduced spectrum width as shown in Fig. 5(d).

4. SINGLE-MCF BIDIRECTIONAL SCN TESTBED AND FEASIBILITY DEMONSTRATION RESULTS

A. Overview of the Bidirectional Single-MCF SCN Testbed

In order to demonstrate the feasibility of single-MCF bidirectional SCNs, we constructed a single-MCF ring network testbed as shown in Fig. 6. The ring network comprises two SXCs based on 19-CF CSSs, which are equipped with $M \times N$ WSSs, and a bidirectional seven-core EDFA (7-C EDFA) with ROIs. Instead of using several 10-km-long 19-CFs expected in real metro and core networks, 2-m-long 19-CF patch cords are used as bidirectional single 19-CF links between the two SXCs and the 7-C EDFA. This is because it is difficult to prepare kilometer-long 19-CFs at this time, and because the main purpose of this experiment is to demonstrate the proof of concept of optical node technology that efficiently accommodates asymmetric traffic. The difference in the number of cores between them is adjusted using a 19-CF FIFO device and 7-CF FIFO device. Seven cores among the 19 cores in the 19-CF CSSs are used in the feasibility demonstration experiments. In the following three sections, detailed descriptions of the key components in the testbed are presented: (i) an any-core-access CSS line-side module, (ii) a specially designed 19-CF employed in the CSS and CS prototypes, and (iii) a bidirectional MC-EDFA prototype with ROIs.

B. Any-Core-Access CSS Line-Side Module Equipped with CSS and CS Prototypes

Figure 7 is a photo of the any-core-access CSS line-side module used in the single-MCF ring network testbed, where a 1×8 19-CF CSS prototype reported in [16] and three 19-CF CS prototypes are equipped in a 19-inch rack mount case together with a controller board and a power supply unit.

The 1×8 19-CF CSS prototype comprises a 3×3 array of 19-CFs, a 3×3 microlens array, a condenser lens, and a 19

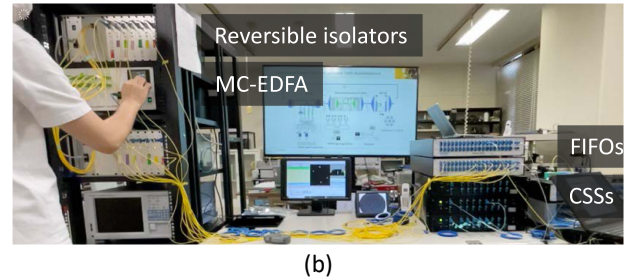
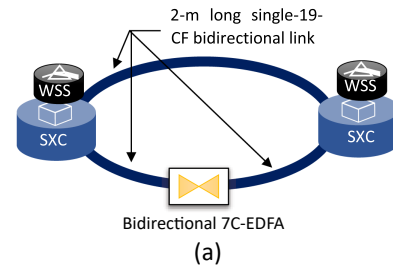


Fig. 6. Implemented single-MCF unidirectional SXC testbed and its key building blocks. (a) Configuration of the single MCF ring network testbed. (b) Single-MCF ring network testbed.

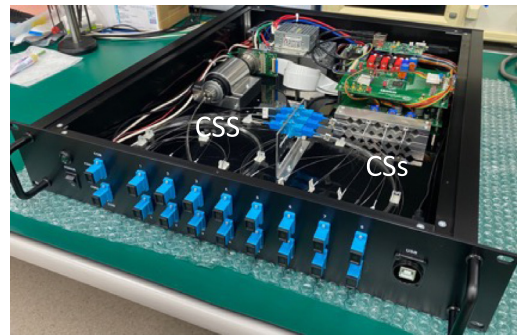


Fig. 7. Any-core-access CSS line-side module equipped with a 19-CF CSS prototype and three 19-CF CS prototypes.

micro-electromechanical systems (MEMS) mirror array, each aligned in a 4-f system. The CSS prototype is packaged in a 44-mm-diameter, 138-mm-long cylindrical housing. The 19 MEMS mirror arrangement is a 180-deg rotation of the core arrangement magnified 62 times, which is determined by the ratio of focal lengths of the collimating lens and the condenser lens used in the CSS. The diameter and spacing of mirrors are 1 mm and 2.46 mm, respectively. The wavelength-swept coupling efficiency measurement from each core in the input 19-CF port to the core with the same core number in eight output 19-CF ports confirmed that the 19-CF CSS has a low insertion loss of less than 4.0 dB over a wide wavelength range of 1500 nm to 1600 nm [16].

Figure 8(a) is a photo of the CS prototype. The CS prototype comprises a standard SMF and a 19-CF, which are arranged adjacent to each other, a condenser lens, and a MEMS mirror each aligned in a simple 2-f system. It is packaged in a 9-mm-diameter, 35-mm-long cylindrical housing. Figure 8(b) shows the insertion loss (IL) characteristics for the connection from the SMF to each core in the 19-CF as a function of the wavelength in the range from 1500 nm to 1600 nm. The IL

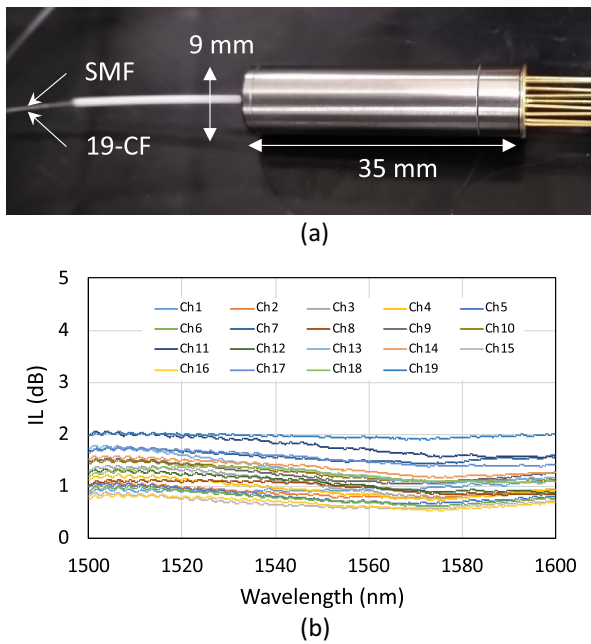


Fig. 8. 19-CF CS prototype and IL versus wavelength characteristics. (a) CS prototype. (b) IL characteristics for the connection from the SMF to each core in the 19-CF as a function of the wavelength.

includes those of FIFO devices used for the launching light from a wavelength-tunable laser diode to each core. An IL of less than 2.0 dB is achieved for all connections across a very wide wavelength range of 100 nm.

C. 19-CF Employed in CSS and CS Prototypes

MCFs are a key component in CSSs and CSs. Since the MCF employed in the CSSs and CSs is used in short lengths and its design requires different considerations than MCFs for long-distance applications, we carefully designed and fabricated a 19-CF for the short-length application. ITU-T Recommendation G.652, which describes the reference characteristics of standard SMFs, defines the cable cut-off wavelength at a fiber length of 22 m. This definition is effective for cabled fibers to ensure single-mode operation. However, when the same fiber is used in shorter lengths, higher-order modes tend to remain in the fiber and cause multipath interference. In addition, the inner core of an MCF tends to have a longer cut-off wavelength due to the influence of the outer core. This means that the cut-off wavelength of a 19-CF for CSS and CS applications must be set to a shorter wavelength than that for the cabled 19-CF. On the other hand, MCFs with a shorter cut-off wavelength tend to have a higher level of inter-core crosstalk (XT) and a higher macro-bending loss. To ensure low macro-bending loss and low XT, we designed the 19-CF so that the cut-off wavelength of the 2-m fiber is less than 1000 nm. Core pitch is another important parameter for both the cut-off wavelength and XT of the inner core. The core pitch is set to 40 μm so that the cut-off wavelengths of the inner and outer cores are the same. A cross-section and characteristics of the fabricated 19-CF are shown in Fig. 9 and Table 1, respectively.

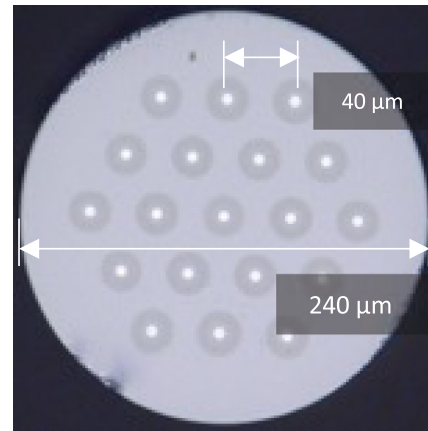


Fig. 9. Cross-sectional photo of 19-CF employed in CSS and CS prototypes.

Table 1. Characteristics of 19-CF

Item	Value
Core pitch	40 μm
Cladding diameter	240 μm
Coating diameter	380 μm
Mode field (1310 nm)	8.5 μm
Diameter (1550 nm)	10.0 μm
Cut-off wavelength	< 1000 nm
XT (2 m) ^a (1550 nm)	-30 dB
Bending loss (1550 nm) (60 nm φ)	< 1 dB/turn

^aXT between two adjacent cores.

D. Bidirectional MC-EDFA Module with ROIs

In this section, the details of the bidirectional MC-EDFA prototypes, which can reconfigure independently the amplification direction of a WDM signal for each core, are described.

1. Configuration and Properties

The bidirectional MC-EDFA prototype is configured by an optical gain block and an amplification direction reconfiguration block as shown in Fig. 10. The optical gain block uses the bidirectional cladding pumping method [8] to amplify all cores of a multicore erbium-doped fiber (MC-EDF) collectively. As is well known [17], optical amplification characteristics of EDFAs depend on the direction of pumping. The use of bidirectional cladding pumping enables the same optical amplification characteristics for all cores even if the direction of amplification is changed for each core of the transmission MCF. The number of cores of the MC-EDF used for this prototype is seven. Hereafter, we refer to this bidirectional MC-EDFA as a bidirectional 7-C EDFA. The amplification direction switching block is constructed of ROIs for a single-core signal. The details of the ROI are given in Fig. 11. Its configuration is very simple, and the reversible function is actualized using a 1×2 optical switch and an optical circulator. The present implementation of single-core-based ROIs is somewhat bulky. However, it is anticipated that more compact

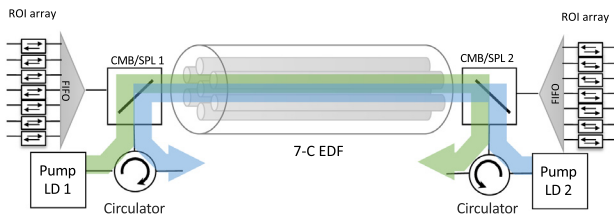


Fig. 10. Configuration of the bidirectional 7-C EDFA prototype.

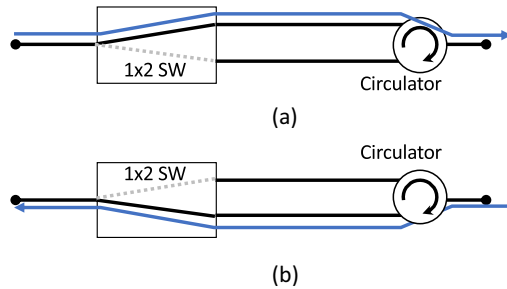


Fig. 11. Configuration of the ROI. (a) West to east. (b) East to west.

Table 2. Details of the Bidirectional 7-C EDFA Prototype

Item	Value
Number of cores	7
Bandwidth	1530–1565 nm
Input power	−5 dBm/core
Maximum pump power	20 W/laser
Pump wavelength	976 nm

implementations will be feasible in the future with the advent of multi-core-based optical switches and circulators.

To evaluate the bidirectional gain block and the direction switching block independently, they are connected using patch fiber cords although they should be spliced ideally to reduce loss, and to avoid unexpected signal reflection between optical connectors, which potentially degrades the amplified signal quality. The IL and inter-core XT due to the reversible isolator are 1.72 dB and 41.3 dB, respectively. The amplification direction can be reconfigured for each core of the optical gain block by controlling, on a core-by-core basis, a 1 × 2 optical switch inside a reversible isolator connected via a FIFO device to the input and output ports of the bidirectional MC-EDFA. Table 2 summarizes the properties of the prototype. A photo of the prototype accommodated in a 19-inch rack case is shown in Fig. 12.

2. Gain and Noise Figure

The amplification characteristics of the bidirectional 7-C EDFA are characterized including the reversible isolators. Figures 13 and 14 show the measured optical gain and noise figure (NF), respectively, under the operation conditions of −5-dBm/core input optical power and 8-W forward pump optical power. The measurement parameter is the core number. Differences of 1.6 dB in gain and 3.3 dB in NF are observed

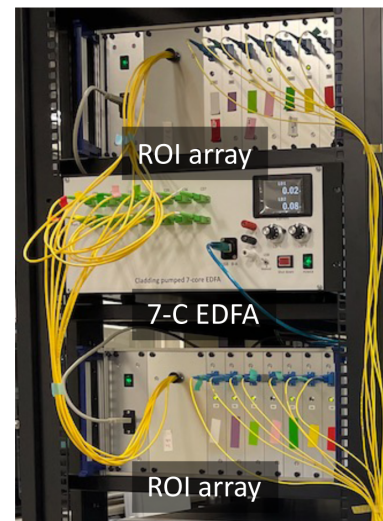


Fig. 12. Bidirectional 7-C EDFA prototype with the amplification direction reconfiguration function for each core.

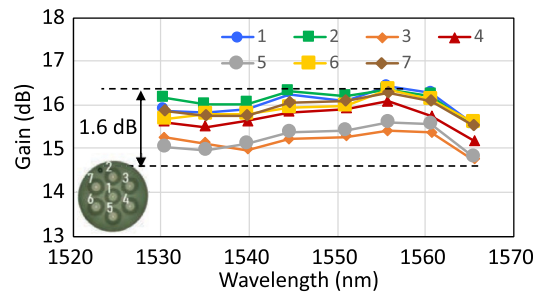


Fig. 13. Core-to-core dependence of gain.

between cores. The measured result of core 1, which is the center core of a 7-CF, is the best among the cores. Since the difference in the IL of the reversible isolators among 7-CF cores is less than 1 dB, it is considered that alignment accuracy of splicing between the 7-CF and 7-C EDF affected the measured results. Since the alignment accuracy of the center core is the best compared to the other cores, core-to-core dependence of the gain and NF will be improved according to the accuracy of the MCF splicing technique in the future. For simplicity, in subsequent evaluations, only core 1, the center core, is discussed since the results of core 1 are the best and the other cores show the same tendency as core 1. As shown in Fig. 14, the measured NF of the bidirectional 7-C EDFA ranging from 7 dB to 10 dB is greater than that of a conventional single-core EDFA of ~5 dB. One reason for this is the larger average ROI insertion loss of 1.2 dB among cores than that for a conventional isolator. Other reasons are the IL of a FIFO device required to implement ROIs and the excess loss associated with splicing 7-CFs, which is currently greater than that associated with splicing conventional SMFs.

Next, we evaluate the amplification direction dependence of the gain and NF. The input optical power is −5 dBm/core. In the case of bidirectional pumping, both forward and backward pump optical power are set identical. The results are summarized in Fig. 15 for gain and in Fig. 16 for NF, respectively. At approximately 20 W of total pump optical power, both

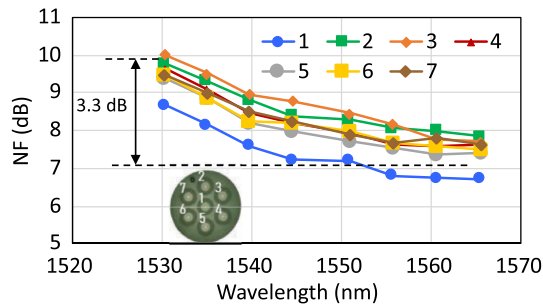


Fig. 14. Core-to-core dependence of the NF.

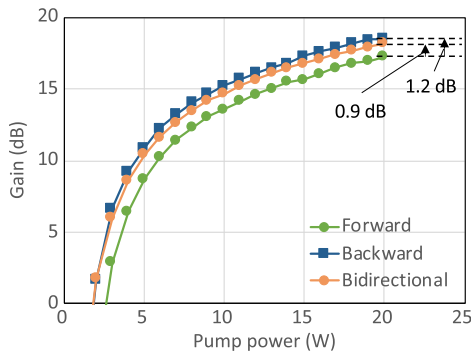


Fig. 15. Pump direction dependence of the gain.

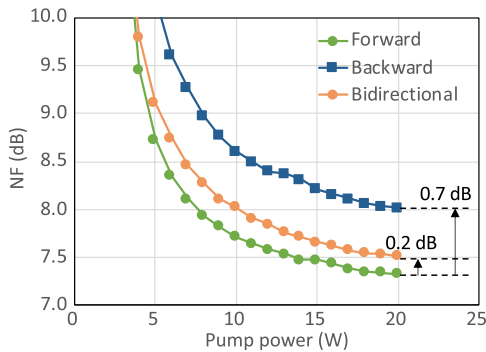


Fig. 16. Pump direction dependence of the noise figure.

gain and NF are measured to become close to saturation for all pump directions. At 20 W of pump optical power, backward pumping exhibits the highest gain and forward pumping yields the best NF characteristics. Bidirectional pumping is the intermediate among the three. This tendency is the same as that for conventional core pumped single-core EDFAs [17]. The important thing is that the NF difference for bidirectional pumping compared to that for forward pumping, which is 0.2 dB, is smaller than that for the backward pumping, 0.7 dB. Therefore, bidirectional pumping is supposed to achieve 1.2-dB greater gain than forward cladding pumping while maintaining almost the same NF at a constant pump optical power. This characteristic is helpful in improving the electric power efficiency of the cladding pumped 7-C EDFA.

E. Detailed Configuration of the Single-MCF Bidirectional Ring Network Testbed

Figure 17 shows the detailed configuration of the single-MCF bidirectional ring network testbed. SXC 1 comprises two 19-CF 1×8 CSS prototypes. Due to the limitation of the available number of CSSs, three CSSs are attached to three of four add/drop ports of one CSS in SXC 1 and a 19-CF FIFO device [18] is attached to the remaining add/drop port. On the client side of SXC 1, a 4×6 MCS is constructed with four 1×6 SPLs and six 1×4 switches. Due to the limitation of the available number of CSSs, SXC 2 is constructed with two 19-CF FIFO devices. A bidirectional 7-C EDFA with ROIs is arranged between SXC 1 and SXC 2. Here, 19-CF FIFO and 7-CF FIFO devices are used for the core number conversion, and 7 of the 19 cores in the SXCs (see inset in Fig. 17) are used in this demonstration.

A pseudo-WDM signal used for the BER versus optical signal-to-noise ratio (OSNR) measurements is created by synthesizing the optical signal generated from a 100-Gb/s dual-polarization quadrature phase shift keying (DP-QPSK) transmitter and the dummy optical signal created by spectrally shaping the amplified spontaneous emission (ASE) light. Seven copies of the pseudo-WDM signal are generated using a 1×8 SPL and delay fiber lines to fill all seven cores in the 7-C EDFA prototype. The bidirectional cladding pump power is controlled to provide an approximate 12-dB gain for each fully loaded C band WDM signal transmitted through each core in the bidirectional 7-C EDFA prototype.

F. Feasibility Demonstration Results

We examined two scenarios: (A) each of three clients requires the entire C band in the west to east (W-to-E) direction and 1/3 of the bandwidth of the C band in the east to west (E-to-W) direction (asymmetric traffic), and (B) each of two clients requires the entire C band in both the W-to-E and E-to-W directions (symmetrical traffic). Figure 17(a) shows the experimental configuration for scenario A, where the three clients are accommodated using four cores by independently allocating the required bandwidth in both directions.

Figure 18(a) shows the BER versus OSNR performance for seven pseudo-WDM signals (comprising a 100-Gb/s DP-QPSK signal and spectrum shaped ASE light as dummy WDM signals), each transmitted through a different core. The inset in the upper left of Fig. 18 shows the intensity distribution of light beams propagating in the W-to-E and E-to-W directions in the A-B plane of the 19-CF in Fig. 17. Each intensity distribution was obtained by disconnecting the 19-CF in the A-B plane and observing the optical beam emitted from the 19-CF connector with an optical beam profiler. It can be confirmed that W-to-E and E-to-W optical signals are propagating in the single 19-CF link as expected. In order to investigate the wavelength dependence of the testbed, BER measurements were performed at the wavelengths of 1541 nm, 1551 nm, and 1561 nm by changing the wavelength of the 100-Gb/s DP-QPSK signal in the pseudo-WDM signals. The figures show that almost no OSNR penalty is observed at the BER of 10^{-3} for all optical signals transmitted through the single-MCF ring network in different cores and different directions

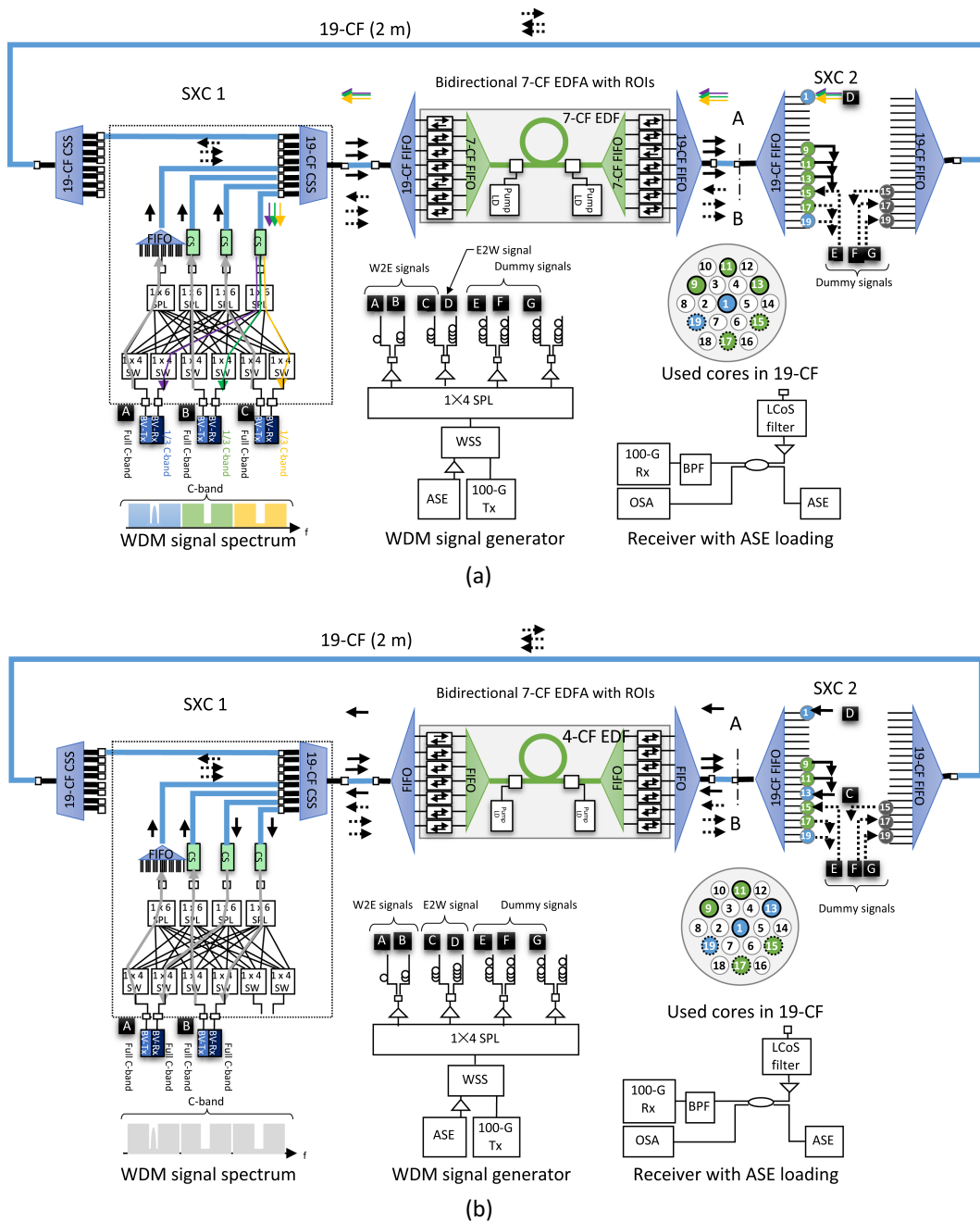


Fig. 17. Single-MCF ring network testbed. (a) Configuration for scenario A (asymmetric traffic). (b) Configuration for scenario B (symmetric traffic).

at different wavelengths. No difference in BER characteristics was observed when changing the wavelength under test in the pseudo-WDM signal. Slight OSNR penalties were observed in the BER versus OSNR characteristics especially in the low-BER region. We believe that this is due to the relatively high level of inter-core XT (-30 dB/2 m, between two adjacent cores) in the 19-CF used in the CSSs, which slightly degrades the BER performance even when the seven cores used were sparsely arranged as shown in Fig. 18. We confirmed that a CSS prototype employing a modified version of the 19-CF having a reduced inter-core XT of <-70 dB/2 m (between two adjacent cores) [19] achieves an aggregated XT from the

other 18 cores of <-42 dB. We expect that the improved CSS will exhibit no OSNR penalty in the BER versus OSNR characteristics even when all 19 cores are lighted. Detailed characteristics of the improved CSS prototype will be reported elsewhere.

We examined symmetric scenario B using the experimental configuration show in Fig. 17(b), where the two clients that require the entire C band for both directions on the route from SXC 1 through the EDFA to SXC 2 are accommodated using four cores. Two are for the W-to-E direction and the other two are for the E-to-W direction. As shown in Fig. 18(b), we confirmed that the single-MCF bidirectional ring network testbed

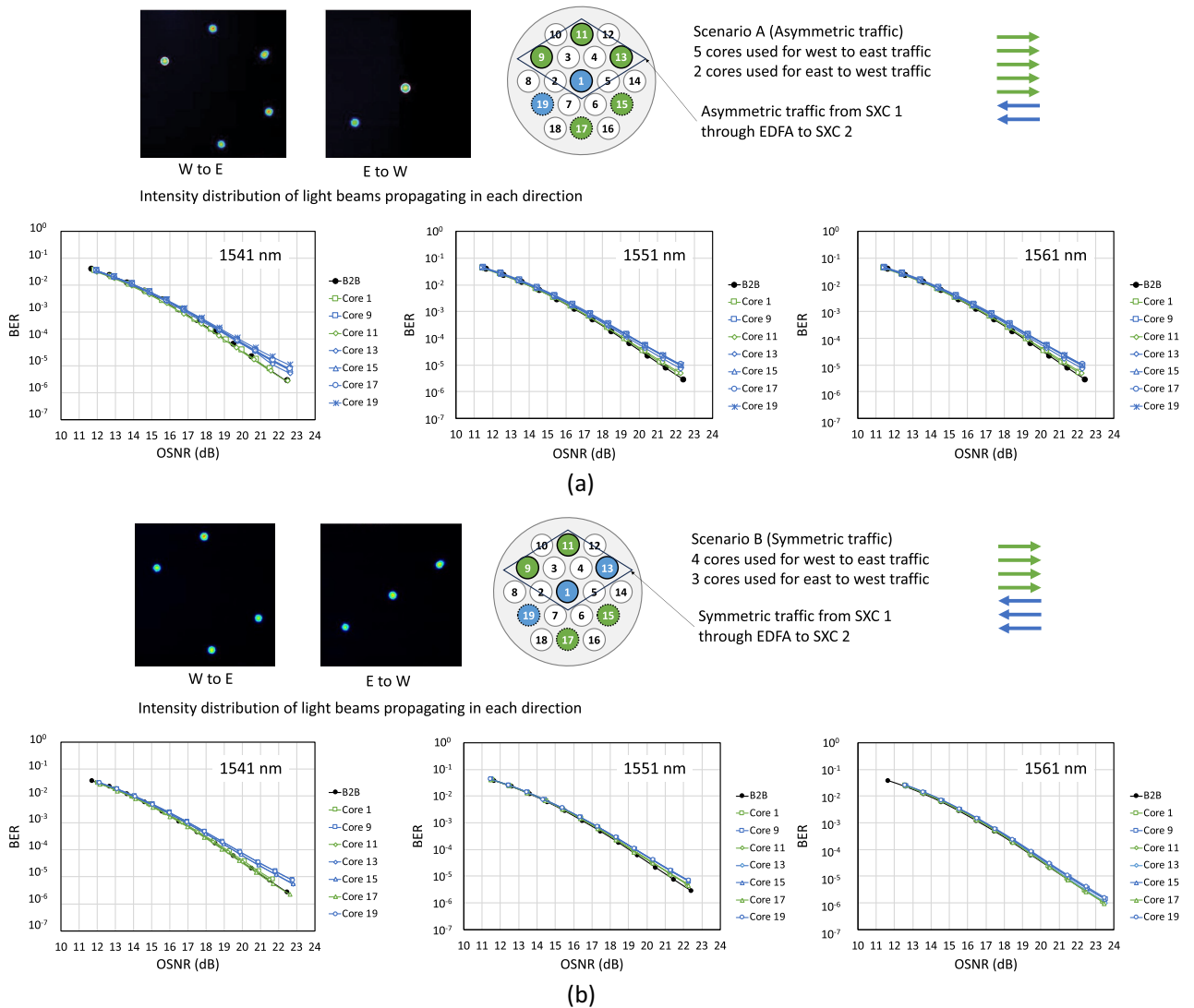


Fig. 18. Experimental results. (a) Scenario A. (b) Scenario B.

exhibits similar BER versus OSNR performance regardless of the symmetry of the accommodated traffic. In general, unidirectional transmission using an uncoupled MCF transmission line suffers from larger inter-core XT than bidirectional transmission resulting in a higher BER [20]. However, since the 19-CF link length between SXCs is as short as 2 m, the difference in symmetry in the signal transmission direction is not expected to cause any difference in BER performance.

5. CONCLUSIONS

In this paper, we proposed a single-MCF bidirectional SCN architecture that efficiently accommodates up and down asymmetric traffic. We presented a feasibility demonstration of the asymmetric bandwidth allocation in a single-MCF SCN by constructing a single-MCF bidirectional ring network testbed that comprises two SXCs based on 19-CF CSSs with an $M \times N$ WSS and a bidirectional 7-C EDFA with ROIs. In the testbed, packaged CSS and CS prototypes equipped into a 19-inch rack mount case were employed. The 19-CF

employed in the CSS and CS prototypes was designed so as to have a sufficiently suppressed higher-order mode even in a shorter length. The bidirectional MC-EDFA prototype has the capability to reconfigure independently the amplification direction of a WDM signal for each core by using an ROI. Experimental results for BER measurements of WDM optical signals traveling different cores in different directions shows there is almost no OSNR penalty for transmission through the single-MCF bidirectional ring network testbed.

In order to achieve a network that can efficiently accommodate asymmetric traffic, it is essential to innovate not only the optical network technology described in this paper, but also technologies in upper layers such as optical transport network (OTN) technology. The authors hope that the proof-of-concept demonstration reported in this paper will be the first step toward such innovation and help promote innovation in the upper layers.

Funding. National Institute of Information and Communications Technology (00201); Japan Society for the Promotion of Science (JP22H01488).

REFERENCES

1. J. M. Simmons, *Optical Network Design and Planning* (Springer, 2014).
2. S. L. Woodward, W. Zhang, B. G. Bathula, G. Choudhury, R. K. Sinha, M. D. Feuer, J. Strand, and A. L. Chiu, "Asymmetric optical connections for improved network efficiency," *J. Opt. Commun. Netw.* **5**, 1195–1201 (2013).
3. B. G. Bathula and W. Zhang, "Breaking the bidirectional link paradigm," in *Optical Fiber Communication Conference (OFC)* (2016), paper Th1E.3.
4. A. M. Saleh and J. M. Simmons, "Technology and architecture to enable the explosive growth of the internet," *IEEE Commun. Mag.* **49**, 126–132 (2011).
5. K. Walkowiak, R. Gościński, and M. Klinkowski, "Evaluation of impact of traffic asymmetry on performance of elastic optical networks," in *Optical Fiber Communication Conference (OFC)* (2015), paper Th11.2.
6. M. Jinno, "Elastic optical networking: roles and benefits in beyond 100-Gb/s era," *J. Lightwave Technol.* **35**, 1116–1124 (2017).
7. E. Riccardi, A. Pagano, and E. Hugues-Salas, "Sliceable bandwidth variable transponders for elastic optical networks: the idealist vision," in *Fotonica AEIT Italian Conference on Photonics Technologies* (2015).
8. D. M. Marom, P. D. Colbourne, A. D'Errico, N. K. Fontaine, Y. Ikuma, R. Proietti, L. Zong, J. M. Rivas-Moscoco, and I. Tomkos, "Survey of photonic switching architectures and technologies in support of spatially and spectrally flexible optical networking [Invited]," *J. Opt. Commun. Netw.* **9**, 1–26 (2017).
9. Y. Matsuno, M. Takahashi, R. Sugizaki, and Y. Arashitani, "Design of 19-core multicore fibers for high density optical wiring," in *27th OptoElectronics and Communications Conference (OECC) and 2022 International Conference on Photonics in Switching and Computing (PSC)* (2022).
10. H. Takeshita, Y. Shimomura, and K. Hosokawa, "Bidirectional cladding-pumped multicore EDFA and its optimization for energy efficiency by tuning pump condition," *J. Lightwave Technol.* **41**, 3455–3461 (2023).
11. M. Jinno, "Spatial channel network (SCN): opportunities and challenges of introducing spatial bypass toward the massive SDM era [Invited]," *J. Opt. Commun. Netw.* **11**, 1–14 (2019).
12. M. Jinno, "Spatial channel cross-connect architectures for spatial channel networks," *IEEE J. Sel. Top. Quantum Electron.* **26**, 3600116 (2020).
13. M. Jinno, I. Urashima, T. Ishikawa, T. Kodama, and Y. Uchida, "Core selective switch with low insertion loss over ultra-wide wavelength range for spatial channel networks," *J. Lightwave Technol.* **40**, 1821–1828 (2022).
14. K. Nakada, H. Takeshita, Y. Kuno, Y. Matsuno, I. Urashima, Y. Shimomura, Y. Hotta, T. Sasaki, Y. Uchida, K. Hosokawa, R. Otowa, R. Tahara, E. Le Taillandier de Gabory, Y. Sakurai, R. Sugizaki, and M. Jinno, "Single multicore-fiber bidirectional spatial channel network based on spatial cross-connect and multicore EDFA efficiently accommodating asymmetric traffic," in *Optical Fiber Communication Conference (OFC)* (2023), paper M4G.7.
15. M. Jinno, T. Ishikawa, T. Kodama, H. Hasegawa, and S. Subramaniam, "Enhancing the flexibility and functionality of SCNs: demonstration of evolution toward any-core-access, nondirectional, and contentionless spatial channel cross-connects [Invited]," *J. Opt. Commun. Netw.* **13**, D80–D92 (2021).
16. Y. Kuno, M. Kawasugi, Y. Hotta, R. Otowa, M. Mizoguchi, F. Takahashi, Y. Sakurai, and M. Jinno, "19-core 1×8 core selective switch for spatial cross-connect," in *27th OptoElectronics and Communications Conference (OECC) and 2022 International Conference on Photonics in Switching and Computing (PSC)* (2023), paper WE3.
17. E. Desurvire, "Analysis of gain difference between forward- and backward-pumped erbium-doped fiber amplifiers in the saturation regime," *IEEE Photon. Technol. Lett.* **4**, 711–714 (1992).
18. K. Watanabe and T. Saito, "Compact fan-out for 19-core multicore fiber, with high manufacturability and good optical properties," in *Opto-Electronics and Communications Conference (OECC)* (2015).
19. K. Nakada, Y. Matsuno, Y. Uchida, M. Takahashi, R. Tahara, T. Izumi, R. Sugizaki, and M. Jinno, "Characteristics and system impact of multipath interference in optical devices with short multicore fibers for spatial channel networks," in *Photonics in Switching and Computing* (2023), paper Fr2A.3.
20. M. Arikawa, T. Ito, E. Le Taillandier de Gabory, and K. Fukuchi, "Crosstalk reduction using bidirectional signal assignment over square lattice structure 16-core fiber for gradual upgrade of SSMF-based lines," in *European Conference on Optical Communication (ECOC)* (2015).

Yosuke Nakada received the B.E. degree in electronics and information engineering from Kagawa University, Takamatsu, Japan, in 2023. He is currently a graduate student at Kagawa University.

Hitoshi Takeshita received the B.E. and M.E. degrees in electrical engineering and information from the University of Tokyo, Tokyo, Japan, in 1993 and 1995, respectively, and the Ph.D. degree in information and communication engineering from the University of Nagoya, Nagoya, Japan, in 2019. In 1995, he joined NEC Corporation, Kawasaki, Japan. His research interests include development of flexible core photonic network technologies and high capacity long-haul optical transmission systems. He is a Senior Member of the Institute of Electronics, Information and Communication Engineers.

Yuki Kuno received the M.E. degree from the Tokyo Institute of Technology, Tokyo, Japan, in 2016. In 2016, he joined santec Co., Aichi, Japan, where he has been engaged in research and development of passive components for optical fiber communication.

Yusuke Matsuno received the B.E. degree from Waseda University in Tokyo, Japan, in 2019 and the M.E. degree from Tokyo Institute of Technology in Tokyo, Japan, in 2021. He joined Furukawa Electric Co., Ltd. in 2021. He has been engaged in research and development of optical fiber technologies. He is currently a member for the Photonics Laboratories.

Itsuki Urashima received the B.E. and M.E. degrees in electronics and information engineering from Kagawa University, Takamatsu, Japan, in 2021 and 2023, respectively.

Yusuke Shimomura received the B.E. degree in applied physics from the Tokyo University of Agriculture and Technology, Fuchu, Japan, and the M.E. degree in basic science from the University of Tokyo, Tokyo, Japan, in 2017 and 2019, respectively. In 2021, he joined the Advanced Network Research Laboratories, NEC Corporation. His research focuses on multicore optical amplifiers.

Yuji Hotta received the B.E. degree from the Aichi Institute of Technology, Aichi, Japan, in 1989. In 1989, he joined santec Co., Aichi, Japan, where he engaged in the design of optical fiber sensing systems. From 2003, he has been engaged in research and development of wavelength tunable laser source systems. Since 2013, he has been engaged in research and development of optical wavelength selective switch systems for ROADM systems.

Tsubasa Sasaki received the M.E. degree from Nihon University in Chiba, Japan, in 2016. He joined Furukawa Electric Co., Ltd., in 2021. He has been engaged in research and development of optical fiber connection technologies. He is currently a member of the Photonics Laboratories. He is a member of the Institute of Electronics, Information and Communication Engineers (IEICE).

Yudai Uchida received the B.E. degree in electronics and information engineering from Kagawa University, Takamatsu, Japan, in 2022. He is currently a graduate student at Kagawa University.

Kohei Hosokawa received the B.E. and M.E. degrees in electronics from the Tokyo Institute of Technology, Tokyo, Japan, in 1999 and 2001, respectively. In 2001, he joined the Media and Information Research Laboratories, NEC Corporation and is currently a director of the Advanced Network Research Laboratories. His research interests include VLSI design technology, free-space optical communication systems, and optical fiber transmission systems.

Ryohei Otowa received the M.E. degree from Chubu University, Aichi, Japan, in 2004. In 2004, he joined santec Co., Aichi, Japan, where he engaged in the design of optical thin films. Since 2008, he has been engaged in research and development of optical switches and equalizers for ROADM systems.

Rika Tahara received the B.E. degree in electronics and information engineering from Kagawa University, Takamatsu, Japan, in 2023. She is currently a graduate student at Kagawa University.

Emmanuel Le Taillandier de Gabory was born in Libourne, France, in 1975. He received the Engineering Diploma from the Ecole Supérieure d'Optique, Orsay, France, in 1999 (now Institut d'Optique Graduate School, Palaiseau, France). From 2000 to 2007, he was with Fujitsu Quantum Device Ltd., Yamanashi, Japan. In 2007, he joined NEC Corporation, Kanagawa, Japan, where he is currently the Director of Advanced Network Research Laboratories. He has been working on transmission technologies for high-capacity long-haul WDM transmission systems, also including SDM transmission systems. He contributed to the world's first demonstration of real-time single-carrier 100G transmission in 2010, to the realization of best in class transpacific QAM systems in 2016, and to the demonstration of the world's largest transmission capacity with standard diameter multicore optical fiber in 2017. He has authored or coauthored more than 50 papers and holds 30 patent applications. He is a Senior Member of the IEICE, Japan. He has been serving as member of the Technical Committee of EXAT, a member of the Technical Program Committees of ECOC, and as a Technical Program Committee category chair of OECC.

Yasuki Sakurai received the M.E. degree in electronics engineering from Tohoku University, Miyagi, Japan, in 2000 and the Ph.D. degree in information processing from Tokyo Institute of Technology, Tokyo, Japan, in 2006. From 2000 to 2003, he worked with Fujitsu Corporation, Kanagawa, Japan, and was in charge of developing optical devices such as LN modulators, silica waveguide devices, and EDFAs for optical fiber communications. In 2006, he joined santec Corporation, Aichi, Japan, where he is currently a director

in the Advanced Optical Components Company. He has been working on research and development of optical functional devices and instruments for optical fiber communications, optical sensing, and optical imaging. He was the recipient of the IEICE Electronics Letter Best Paper Award in 2000.

Ryuichi Sugizaki (M'15) received the B.E. degree from the Chiba Institute of Technology, Chiba, Japan, in 1990. In 1990, he joined Furukawa Electric Co., Ltd., Tokyo, Japan, where he has been engaged in research and development of optical fibers. He is currently a specialist for the Telecommunication and Energy Laboratories. He is a Senior Member of the Institute of Electronics, Information and Communication Engineers (IEICE). He was the recipient of the Outstanding Poster Paper Award of International Cable Connectivity Symposium in 2017.

Masahiko Jinno (M'90–SM'12–F'20) received the B.E. degree and M.E. degree in electronics engineering from Kanazawa University, Ishikawa, Japan, in 1984 and 1986, respectively, and the Ph.D. degree in engineering from Osaka University, Osaka, Japan, in 1995 for his work on ultra-fast optical signal processing based on nonlinear effects in optical fibers. He currently serves as a Professor in the Faculty of Engineering and Design at Kagawa University, Takamatsu, Japan. His current research interests include architecture, design, management, and control of optical networks, optical transmission systems, optical cross-connects, optical switches, and rate- and format-flexible optical transponders. Prior to joining Kagawa University in October 2012, he was a Senior Research Engineer and Supervisor at Nippon Telegraph and Telephone (NTT) Network Innovation Laboratories, NTT Corporation, conducting pioneering research on spectrum- and energy-efficient elastic optical networks (EONs). From 1993 to 1994, he was a guest scientist at the National Institute of Standards and Technology (NIST), Boulder, Colorado, USA. He authored or co-authored over 200 peer-reviewed journal and conference papers in the fields of ultra-fast optical signal processing for high-capacity optical time division multiplexed transmission systems, optical sampling and optical time-domain reflectometry, ultra-wideband WDM transmission systems in the L-band and S-band, ROADM systems, GMPLS and application-aware optical networking, EONs, and spatial channel networks (SCNs). Dr. Jinno is a Fellow of the Institute of Electronics, Information and Communication Engineers (IEICE) and a Senior Member of Optica. He received the Young Engineer's Award in 1993, the Best Tutorial Paper Awards in 2011 and 2021, the Best Paper Award in 2012, the Achievement Award in 2017, and the Milestone Certificate in 2017 from the IEICE; the Best Paper Awards from the 1997, 1998, 2007, and 2019 Optoelectronics and Communications Conferences (OECC); the Best Paper Award from the 2010 ITU-T Kaleidoscope Academic Conference; and the Outstanding Paper Award in 2013 from the IEEE Communications Society Asia-Pacific Board.